Composition effects of electrodeposited Cu-Ag nanostructured electrocatalysts for CO_2 reduction

Elena Plaza-Mayoral[1], Valery Okatenko[2], Kim N. Dalby[3], Hanne Falsig[3], Ib Chorkendorff[4], Paula Sebastián-Pascual[*1], María Escudero-Escribano[*,1,5,6]

(1) Center for High Entropy Alloy Catalysis, Department of Chemistry, University of Copenhagen, Universitetsparken 5, 2100 Copenhagen, Denmark

(2) Laboratory of Nanochemistry for Energy Research, Institute of Chemical Sciences and Engineering, Ecole Polytechnique Fédérale de Lausanne, Sion CH-1950, Switzerland

(3) Topsoe A/S, Haldor Topsøe Allé 1, DK-2800 Kgs. Lyngby, Denmark

(4) Department of Physics, Surface Physics and Catalysis, Technical University of Denmark, Fysikvej, DK-2800 Lyngby, Denmark

(5) Catalan Institute of Nanoscience and Nanotechnology (ICN2), CSIC, Barcelona Institute of Science and Technology, UAB, 08193 Bellaterra, Barcelona, Spain

(6) Catalan Institution for Research and Advanced Studies (ICREA), Pg. Lluís Companys 23, 08010 Barcelona, Spain

*Corresponding authors:

E-mail: maria.escudero@icn2.cat

E-mail: paula.pascual@chem.ku.dk

ABSTRACT

The electrochemical reduction of carbon dioxide (CO_2RR) to valuable C_{2+} liquid fuels and oxygenates, such as ethanol and propanol, is a promising strategy to minimize the carbon footprint and store renewable electricity. In this study, we investigate the CO_2RR on electrodeposited Cu-Ag nanostructures obtained using a green choline chloride and urea deep eutectic solvent (DES). We show that Cu-Ag nanostructured electrocatalysts with tunable composition, loadings, and size can be simply prepared in one step, without adding other additives or surfactant agents. We investigate the intrinsic activity and selectivity of the CO_2RR by determining the electrochemically active surface area (ECSA) using lead underpotential deposition (UPD). The analysis of the partial current densities normalized by the ECSA shows that the addition of Ag on electrodeposited Cu primarily suppresses the production of hydrogen and methane with respect to Cu nanostructures. At the same time, the production of carbon monoxide (CO) slightly increases but, the partial current of the total C_{2+} products does not considerably increase. Despite that the production rate of C_{2+} is similar on Cu and CuAg, the addition of Ag enhances the formation of alcohols and oxygenates over ethylene, in line with previous reports. We highlight the potential of metal electrodeposition from DES as a sustainable and inexpensive strategy for the development of bimetallic Cu-based nanocatalysts towards CO_2RR.

Keywords

Electrodeposition, electrocatalysis, CO_2 reduction, deep eutectic solvent, copper-silver nanostructures.

Table of contents graphic

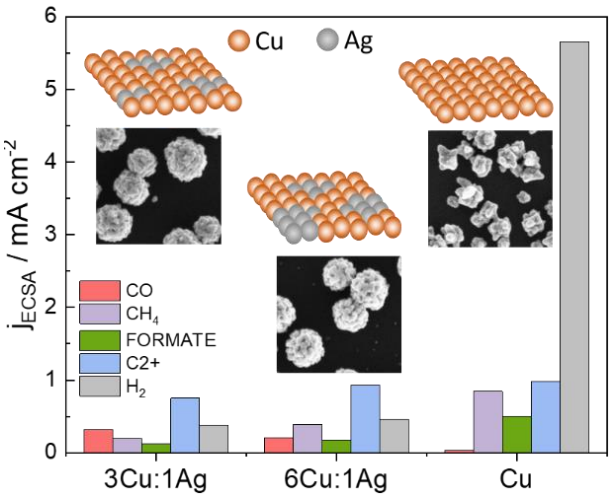

Introduction

To reduce the negative effect of greenhouse gas emissions such as carbon dioxide, a broad range of mitigation strategies coupled with renewable energy have been intensively investigated in the last decade.[1] The electrochemical reduction of carbon dioxide (CO_2RR) is a long-term solution to produce renewable chemicals and fuels, and close the unbalanced carbon cycle.[2–5] In particular, the design of new catalyst structures to convert CO_2 molecules into renewable liquid fuels such as ethanol and propanol has gained increasing interest. These green fuels are compatible with current energy infrastructure, can be used in transportation, and are easily and safely stored and transported.[6–11]. Moreover, the CO_2RR also produces other minor products, such as acetate, acetaldehyde, or ethylene glycol which are building block molecules used in industry to produce further long-chain carboxylates or bio-based chemicals.[12–17]

Copper and Cu-based materials have been the most investigated metallic electrocatalysts for the CO_2RR as they can reduce CO_2 beyond CO and HCOOH and produce valuable multi-carbon products.[6,18,19] Even though pure copper is capable of converting CO_2 to C_{2+}

products with relatively high activities, the reaction is still limited due to the competing hydrogen evolution reaction (HER) and the low product selectivity. The reduction of CO_2 to C_{2+} products on copper is mainly limited to ethylene (C_2H_4), whereas other C_2 or C_3 products such as ethanol and propanol are often generated in lower amounts.[20] The formation of ethylene and ethanol occurs via a C-C coupling reaction of two adsorbed CO molecules which leads to a common hydrogenated dimer intermediate.[8] This intermediate first evolves into ethylene and then is converted into ethanol after subsequent hydrogenation steps, or to propanol if a third CO molecule is inserted.[21] As the number of electrons required to produce alcohols on copper is higher than to produce ethylene, ethylene is generally favored on copper except on some specific surface structures or single facets.[13,22–24]

Different strategies and types of copper-based surfaces with tailored structure and composition have been prepared aiming to switch selectivity towards oxygenates and alcohols over ethylene. The first strategy relies on tuning the surface structure or the shape and size of the nanoparticles. Copper nanocubes of 44 nm with more (110)/(100) steps edges were found to favor the C-C coupling enhancing the selectivity towards C_2H_4 up to 40% and over a 10% of C_2H_6O and C_3H_8O.[25] Recently, Aran-Ais et. al. have also shown how applying pulses to Cu(100) changes the surface structure increasing the production of ethanol to near 30%, similar to the Cu(310) facet reported by Hori and co-workers.[26,27] Another strategy is based on tandem catalysts, i.e. the reaction occurs in two steps catalyzed by two different metals[18,28,29] Jaramillo et. al. presented a tandem catalyst of Au NPs on a polycrystalline Cu foil, in which gold increased the CO concentration on the surrounding copper, where the CO was selectively reduced to alcohols.[28] Finally, tuning the electronic structure by metal alloying allows to favor alcohols production over C_2H_4, e.g., by combining Cu with Zn, Pd or Ag.[30–33] In particular, Cu-Ag are promising bimetallic catalysts to reduce CO_2 to liquid and

oxygenated products such as ethanol, propanol, acetaldehyde and ethylene glycol as both tandem catalysts and alloys.[29,34–36]

On one side, pure Ag electrocatalysts are typically selective towards CO production under CO_2RR conditions.[37] Previous studies have shown how mixing Cu and Ag enhances the production of C_{2+} products by increasing the CO coverage on the surface or by blocking specific sites that might produce the competing H_2 instead.[29,38,39] A study on copper-silver composites suggested that the CO availability is key to enhance the ethanol production, either by *CO dimerization or via an alternative open pathway of *CO and *CH_x coupling.[36] Cu-Ag tandem catalysts also confirmed facet-dependent production of ethanol via *CO - *CH_x coupling at edges and corner sites adjacent to Ag atoms because of the *CO enrichment on the surface.[29] On the other hand, a study on CuAg surface alloys presented the formation of multi-carbon oxygenates due to compressive surface strain of the Cu atoms which selectively suppresses the HER by weakening the adsorption energy of *H.[38] On a similar basis, through a compressive strain and reduced electron density, CuAg multi-phase alloys were also proved to be promising catalysts for the production of acetaldehyde.[35]

These Cu-Ag catalysts for CO_2RR have been prepared through different chemical and physical synthesis methods over the years.[38,40] Colloidal synthesis has been widely employed for the preparation of NPs followed by their deposition onto the chosen substrate.[29,41] However, they usually need surfactant agents or additives to control the growth of the NPs, which might adhere on the surface inhibiting the electrocatalytic response, meaning that they need to be removed in subsequent time and energy-consuming cleaning steps.[42] Co-sputtering of the metals allows for the preparation of surfaces with controlled composition and has been further scaled, although it requires the use of ultra-high vacuum which consumes a high amount of energy.[8] Metal electrodeposition in green non-aqueous solvents has emerged as an easy alternative for the preparation of new bi- and multi-metallic nanostructures.[43,44]

Electrodeposition is a versatile and affordable technique widely employed in the plating industry to prepare a broad range of materials such as metallic nanoparticles and think films, metal oxides, composites, and alloys.[45] Metal electrodeposition in deep eutectic solvents (DES) offers several advantages in contrast to aqueous media. DES present a wider electrochemical window, good conductivity, and good stability, they do not require the addition of any surfactants for a controllable deposition, they are soluble in water, non-toxic, and facilitate the preparation of deposits with a homogenous distribution over the substrate surface.[44,46–50]

In this paper, we use our sustainable and simple method from a choline chloride urea DES to prepare electrodeposited Cu-Ag bimetallic nanostructured catalysts for CO_2RR.[51] We have prepared Cu and Cu-Ag nanostructures and rationally assessed how the introduction of silver changes the product selectivity and intrinsic activity toward CO_2RR. We have used two different bath compositions and prepared different loadings to evaluate how small changes in surface morphology, size of the nanostructures, and composition affect the performance. We have evaluated our nanocatalysts for the CO_2RR at different potentials in terms of product selectivity. We have addressed how different Ag/Cu ratios influence the production of oxygenates over ethylene, as well as the formation of hydrogen in the competing HER reaction of our electrodeposited CuAg nanostructures. Finally, although CuAg produces valuable oxygenated compounds, selectivity varies significantly between different reports, likely due to the sensitivity of the reaction to composition, size, or morphology of the catalyst.[38] In this regard, we want to highlight the importance of estimating the electrochemically active surface area (ECSA) to separate the effects of having different structures and large areas in nanoparticles and nanostructures from their intrinsic catalytic performance.[6] We have recently shown that one valuable method to estimate the ECSA of copper and copper-based catalysts is to record the voltammetric lead underpotential deposition (UPD) on copper.[52]

Lead UPD provides intense and reversible features that correspond to the reversible adsorption/desorption of a sub-monolayer of lead on copper and silver, thus providing quantitative information on the number of surface active sites per unit area.[53,54] Thus, we have determined the ECSA by using lead UPD to rationally address how the addition of different amounts of silver modifies the intrinsic partial currents of the products formed during the CO_2 conversion.

2. Experimental section

Preparation of the nanostructured Cu-Ag deposits from DES:

The metal salts $CuCl_2$ (Sigma-Aldrich, 99 %) and AgCl (Sigma-Aldrich, 99 %) were dissolved in a 1:2 choline chloride (ChCl, Across Organics, 99 %) and urea (Sigma-Aldrich, 99 %) DES under magnetic stirring at 60°C following the procedure of precious publications.[46,52] Three different baths were prepared for the electrodeposition of the metallic nanostructures: (a) 0.075 M $CuCl_2$ / 0.025 M AgCl + DES solution, corresponding to 3Cu:1Ag molar ratio solution; (b) 0.086 M $CuCl_2$ / 0.014 AgCl + DES solution, corresponding to 6Cu:1Ag molar ratio solution; (c) 0.1 M $CuCl_2$ + DES solution. Prior to the electrodeposition, the bath solutions were dried with a N_2 or Ar stream for several hours to avoid the solvent co-reduction and reduce the quantity of water on the solvent, facilitating the deposition.[55]

We performed the electrodeposition process by applying a constant potential until we reached a specific charge by chronoamperometry on a thermostatic three-electrode glass cell with a PTFE cap as shown in Figure 1S of the Supplementary Information (S.I). The counter electrode for the Cu-Ag baths was a Pt wire, while we used a Ag wire as pseudo reference electrode. Both were pre-treated by flame-annealing and rising with ultrapure water (Sartorius Arium Pro). When necessary, a 10 % diluted HNO_3 solution (Sigma-Aldrich) was used to remove metallic traces. For the single Cu solution in DES, copper wires were used both as counter and

pseudo reference electrodes. Here, they were pre-treated with a 10 % diluted HNO_3 solution and rinsed abundantly with ultrapure water. The working electrodes (WE) were Glassy Carbon (GC) plates of 25*25 mm^2 and 3 mm thickness, one side diamond polished to mirror finish (SIGRADUR G plates, HTW GmbH). All potential values were referenced against the Ag | AgCl scale. Right before the electrodeposition, the GC electrodes were prepared by polishing with water-based α-alumina powder of 0.3 and 0.05 μm coarseness (Struers). Subsequently, they were rinsed and sonicated with ultrapure water to remove all alumina traces and dried with N_2 stream. The temperature of the DES baths was always kept at 70°C with a water bath to reduce the viscosity increasing the deposition rates and avoiding the solvent co-reduction.[55] For the measurements and analysis, we used a NOVA potentiostat and software.

CO_2 electroreduction (CO_2RR) measurements and analysis:

The electrochemical reduction of CO_2 was evaluated at ambient pressure CO_2 in a customized polycarbonate H-cell fitted with Buna-N O-rings.[29,56] The chosen electrolyte was a 0.1 M $KHCO_3$ obtained by bubbling CO_2 (Carbagas, 99.999%) through 0.05 M K_2CO_3 (Acros Organics, 99+ %,) solution for 1 h. Each measurement was analyzed using a Biologic SP-300 potentiostat in a chronoamperometry regime for one hour at applied potentials between -0.8 V_{RHE} and -1.3 V_{RHE}. We calculated the ohmic drop at each sample by electrochemical impedance spectroscopy (EIS) and corrected the chronoamperometry potential following the equation $E = E_{ap} - iR_{\Omega}$. The reference electrode was a Ag | AgCl electrode (Innovative Instruments, Inc) which was tested against the master electrode prior to the measurements, and the measured voltages were then converted to the reversible hydrogen electrode scale (RHE). The working electrodes were the electrodeposited Cu and CuAg nanostructures on the GC electrodes. The geometric area in contact with the solution was 1.39 cm^2. The counter electrode was a Pt foil pre-treated by flame-annealing and rinsing with ultrapure water. Both working

and counter electrode were positioned in parallel to allow uniform potential distribution. The anion exchange membrane separating the catholyte from the anolyte was a Selemion AMVN. Each compartment was filled with 2 mL of electrolyte solution. During reaction, the electrolyte of both compartments was constantly bubbled with CO_2 at a flow of 5 sccm to keep the solution saturated with CO_2, ensure that CO_2 reaches the electrode surface, and allow a continuous analysis of the gas products through the on-line gas chromatograph. The gas products were detected by the SRI 8610C gas chromatograph (GC) with a HayeSep D porous polymer column, thermal conductivity detector, flame ionization detector and, nitrogen (99.999 %) as the carrier gas. Then, the calibration curves from standard gas mixtures were employed to calculate the concentration of each gas product. The liquid products were analyzed by high-performance liquid chromatography (HPLC) on a Thermo Scientific UltiMate 3000 instrument. The eluent for the HPLC analysis was a 5 mM H_2SO_4 solution.

Pb underpotential deposition (UPD) and estimation of the ECSA and Roughness factor:

The Pb-UPD measurements were carried out on a three-electrode cell like the one used for the electrodeposition. We used a solution of 2 mM $Pb(ClO_4)_2$ (Sigma-Aldrich, ≥ 99.995 %) + 0.1 M $KClO_4$ (Sigma-Aldrich, ≥ 99.99 %) + 1 mM $HClO_4$ (suprapur 70 %, Merck) in milli-Q (18.2 MΩcm, TOC < 5 ppm) water. The counter and reference electrodes were the same as for the electrodeposition experiments. The working electrodes were our deposited Cu and Cu-Ag nanostructures on the GC. UPD is a surface process sensitive to the structure and real area of the catalysts as reported in previous works.[46,52,53] By integrating the involved charges of the anodic and cathodic voltammetric scans of the Pb UPD cyclic voltammograms (CVs), we can estimate the ECSA and roughness factor (R) of our nanostructures. An average from the anodic and cathodic integrated charges is used for the calculations since UPD is a reversible process.

Morphological and compositional analysis:

Three different scanning electron microscopes (SEM) were used for the morphological analysis of our nanostructures before and after reaction. A JEOL 7800-F prime SEM housed at the Niels Bohr Institute at the University of Copenhagen, a high-resolution Zeiss Gemini 500 field-emission scanning electron microscope (FE-SEM) at Topsoe S/A, and a Thermo-Fisher Teneo using an in-lens (Trinity) detector at Ecole Polytechnique Fédérale de Lausanne (EPFL). The first two microscopes were used to acquire the images with a beam energy of 2 kV while the third used 5 kV.

The energy-dispersive X-Ray spectroscopy (EDS) analysis was carried out on two different microscopes using two different EDS detectors. A Thermo Scientific UltraDry silicon drift detector with Pathfinder Software was used for the EDS acquired from Topsoe, and a Bruker XFlash Silicon drift EDX detector with Esprit software was used for the EDS analysis performed at EPFL. In both cases, accelerating voltage of 15 kV was used to collect the EDS data.

For a more insightful surface composition analysis, X-ray Photoelectron spectroscopy (XPS) was performed at the Technical University of Denmark (DTU) by a Theta Probe instrument (Thermo Scientific) using an Al anode X-ray source (Kα line = 1486.6 eV). The XPS chamber's base pressure was $< 5.0 \times 10^{-8}$ mbar. All measurements used a X-ray beam size of 400 μm and a pass energy of 100 eV. Each survey recorded 20 scans while each element spectra recorded 50 scans. We carried out a depth analysis by sputtering (4 kV and 1.0 μA) with N6 Ar (1.1×10^{-7} mbar) the samples for 40 seconds, 20 seconds per level. The spectra were recorded on each level, where level 0 means no sputtering. After the survey scans, C1*s*, O1*s*, Cu2*p*, and Ag3*d* peaks were measured in steps of 0.1 eV. We used Thermo Avantage Software for the data acquisition and analysis with a Shirley type background for all instances.

3. Results

To assess how the Ag/Cu ratio in the nanostructures affect the CO_2RR, we electrodeposited bimetallic nanostructured electrocatalysts with tunable composition by using two different bath compositions: 0.075 M $CuCl_2$ / 0.025 AgCl + DES solution and 0.081 M $CuCl_2$ / 0.014 AgCl + DES solution. We named the nanostructures prepared from these solutions as 3Cu:1Ag and 6Cu:1Ag respectively, in which the number indicates the 3:1 and 6:1 molar ratio from the bath solution of Cu and Ag, respectively. Pure Cu nanostructures were also prepared from a 0.1 M $CuCl_2$ + DES solution and compared with the CuAg nanostructures. We have characterized our systems by cyclic voltammetry (CV) and chronoamperometry (CA) to evaluate the optimal potential range to perform the electrodeposition on a glassy carbon. In this range, the current-time CA transients exhibit the characteristic shape of a nucleation and growth mechanism (Fig 2SA and 2SB).[48,52,57] We prepared the deposit at moderate rates by applying a moderate applied overpotential in between the optimal range. For the Cu-Ag systems, at electrodeposition applied potentials between -0.7 $V_{Ag|AgCl}$ and -0.8 $V_{Ag|AgCl}$ we obtain a homogeneous and stable surface, whereas high applied overpotentials lead to poorly adherent deposits. A detailed description of the electrochemical characterization is explained in the Supporting Information (S.I). The 3Cu:1Ag deposits were prepared at a potential of -0.75 $V_{Ag|AgCl}$, the 6Cu:1Ag deposit at a potential of -0.73 $V_{Ag|AgCl}$, and the single Cu deposits at a potential of -1.05 $V_{Ag|AgCl}$. At these applied potentials, solvent co-reduction does not overlap with the metal electrodeposition. Therefore, we have assumed that the electrodeposition has an efficiency of 100% and all the circulated charge is related to the reduction of the metal ions in solution.

We prepared nanostructures with three different loadings by controlling the time of deposition and circulated charge, aiming to address how the loading influences the morphology, size, and composition of the nanostructures. We deposited nanostructures on the glassy carbon with 5.29

cm^2 area using three circulated charges: Q = -200 mC, -270 mC, and -485 mC. Then we characterized the CuAg nanostructures using SEM, XPS, and EDS. Figure 1A and Figure 1B illustrate the characterization of 3Cu:1Ag at -200 mC and -485 mC respectively. We observed rounded and rough Cu-Ag NPs. Figure 3S also shows higher-resolution SEM images of the three loadings in which we can relate the roughness with visible porosity. At high coverages, the nanoparticles become slightly bigger (from 200 nm up to 400 nm) likely due to surface diffusion and progressive electrodeposition. The XPS spectrum of the 3Cu:1Ag sample at -485 mC (Fig. 7SA and 7SB) shows that the surface composition is 1:1 after applying 20 seconds of sputtering to remove any traces of contamination. All details from the XPS measurements are explained in the S.I. The EDS color maps show how both metals are distributed all over the substrate with a bulk composition of 1.8:1 of Cu and Ag. We have calculated the mass loadings based on the EDS results using Faraday's law. We have obtained a mass loading of 0.1 mg for -200 mC, 0.14 mg for -270 mC, and 0.24 mg for -485 mC, which equals 19, 26, and 45 μg cm^{-2}, respectively. The EDS results have confirmed that the composition of the deposits in bulk does not change while increasing the loading and there is only a change in the NPs size. We ascribe these results to the fact that the deposition rates of Cu and Ag are similar and both metals are well-mixed in the bulk. However, the surface composition could change due to the lower surface energy of silver or because of air exposure or dissolution/redeposition of copper after bringing the nanostructures to open circuit potential.[58–60]

Before testing these nanostructures for CO_2RR, we have determined the ECSA and roughness factor (R) of each sample using voltammetric lead UPD, to assess their intrinsic activity or activity normalized by surface active sites during the CO_2RR. The roughness factor (R) gives us the increase in the active area in relation to the geometric area.[61,62] Figure 1C shows the Pb UPD voltammograms of the 3Cu:1Ag nanostructures from Figure 1A (black line) and 1B

(blue line). The lead UPD on the 3Cu:1Ag nanostructures shows a pair of quasi-reversible peaks, a single broad and intense peak centered at 0.12 V_{RHE} in the cathodic scan, with its counterpart at 0.15 V_{RHE} in the anodic scan. The lack of sharp peaks indicates that we most likely have deposited polycrystalline structures.[53] The Pb UPD current intensity increases with the loading as well as with the size of the nanostructures, indicating that the larger nanostructure deposited at -485 mC has a higher roughness factor than the sample at -200 mC. The calculated ECSA and R are 4.86 cm^2 and 0.92 for the black line and, 8.18 cm^2 and 1.54 for the blue line, respectively. The fact that the R is close to one in both cases is likely because we are only depositing a few dispersed nanostructures on the glassy carbon without covering the substrate.

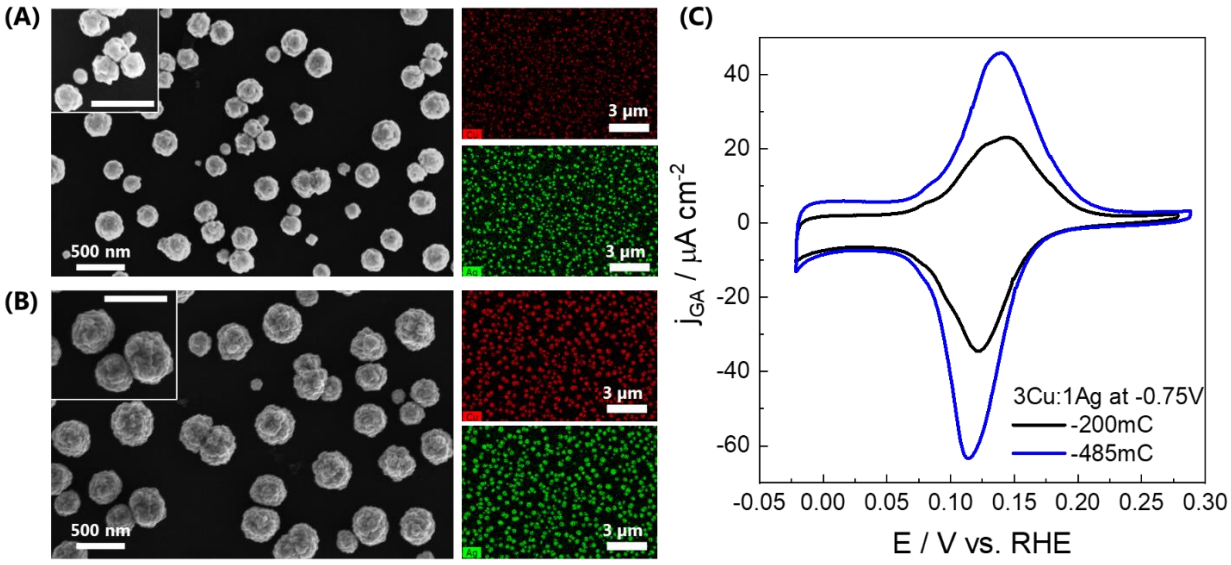

Figure 1. Characterization of the CuAg nanostructures before reaction: SEM of 3Cu:1Ag at -0.75 $V_{Ag\,|\,AgCl}$ and **(A)** -200 mC, and **(B)** -485 mC with the corresponding EDS maps. The scale bars on the inlet SEM images correspond to 500 nm. **(C)** Lead UPD of the nanostructures at (A) and (B). The pH of the Pb UPD electrolyte is 3.2.

After preparing the 3Cu:1Ag nanostructures, we tested their performance toward CO_2RR in a 0.1 M $KHCO_3$ solution, using an H-cell setup connected to the online GC to investigate the product selectivity, as described in the Experimental section. First, we investigated the product

distribution at different reaction potentials from -0.8 V_{RHE} to -1.2 V_{RHE}. Figure 2A shows the faradaic efficiencies and current densities normalized by the ECSA of the 3Cu:1Ag deposit at -485 mC. The data from the deposits at -200 mC and -270 mC is illustrated in Figure 8S of the S.I. At the lowest overpotential of -0.8 V_{RHE}, we only obtain H_2, CO, and formate, whereas no liquid multi-carbon products are detected. At -0.9 V_{RHE}, the H_2 already drops to 13%, the CO production increases to 55% and we start detecting C_{2+} products i.e., C_2H_4 and acetate. The intermediate overpotentials of -1.0 V and -1.1 V_{RHE} are the optimal potentials to produce liquid C_{2+} products since H_2 stays under 23%, the production of CO is reduced and C_2H_4 increases together with the production of liquid C_{2+} products. When adding Ag to the Cu, the competing HER is suppressed between -0.9 V_{RHE} and -1.1 V_{RHE}. Our results align with other works reported in the literature on Cu-Ag catalysts which also show a decrease of the H_2, and an increase in the production of both CO and liquid oxygenates (acetaldehyde, ethanol, and propanol) compared to single copper NPs.[20,36,38,63] For higher overpotentials, H_2 drastically doubles its value and the CH_4 production becomes dominant as occurs on pure copper.[36,64]

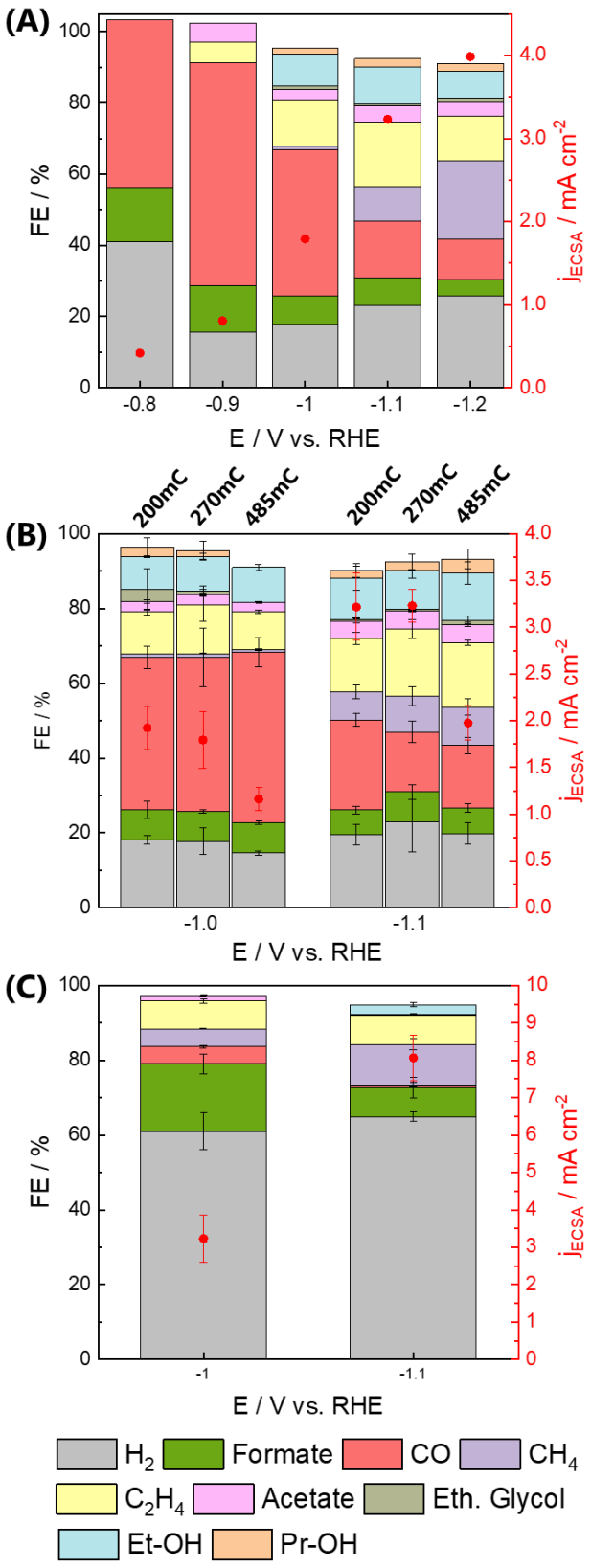

Figure 2. Product selectivity of 3Cu:1Ag during 1h of CO_2RR **(A)** depending on the potential (from -0.8V_{RHE} to -1.2V_{RHE}) at -485 mC and, **(B)** the optimal potentials (-1.0V_{RHE} and -1.1 V_{RHE}) for the three coverages (-200 mC, -270 mC and -485 mC). **(C)** Product selectivity of Cu nanostructures at -485 mC and the optimal potentials after 1h CO_2RR.

We have addressed the catalytic performance of our deposited nanostructures at the applied potentials of -1.0 V_{RHE} and -1.1 V_{RHE} and under one hour of CO_2RR, to assess the selectivity changes of ethylene versus liquid C_{2+} products, as well as the stability of the nanostructures. Figure 2B represents the faradaic efficiencies and normalized current densities of the 3Cu:1Ag at the three prepared loadings of -200 mC, -270 mC, and -485 mC. We present the average of three different measurements of each sample with their corresponding standard deviations from triplicate measurements. For a more in-depth analysis, we have summarized in the S.I. the average faradaic efficiencies (%) and the intrinsic partial currents normalized by the ECSA (mA cm^{-2}) in Table S2, Table S3 and Table S4 for -200 mC, -270 mC and -485 mC, respectively. The three samples exhibit a similar product selectivity which we attribute to the fact that the surface and bulk composition are similar. Only the sample at -485mC shows a slight decrease in intrinsic activity which could be related with the differences in size and structure. At both potentials, the H_2 keeps suppressed below 23% while the CO goes up to 46 % at -1.0 V_{RHE} and decreases to between 16 and 24% at -1.1 V_{RHE}. Ethanol is the most produced liquid C_{2+} product. Both ethylene and ethanol are more favored at -1.1 V_{RHE} with an average of 16% C_2H_4 and 12% C_2H_6O in contrast to 11% and 9% at -1.0 V_{RHE}. The other liquid C_{2+} products, i.e., propanol, acetate, and ethylene glycol vary in low proportions between both potentials. The production of liquid C_{2+} products reaches 20% at -1.1 V_{RHE} while it remains at 17 % at -1.0 V_{RHE}. However, if we evaluate the relationship between C_{2+} products and ethylene, the liquid C_{2+}/C_2H_4 ratio is 1.5 at -1.0 V_{RHE} while it is 1.2 at -1.1 V_{RHE}. Our production distribution results and the intrinsic currents after one hour of CO_2RR at the 3Cu:1Ag nanostructures are close to the values of several Cu-Ag systems from the literature.[35,36] We observed that the H_2 and the CO production drops down whereas the C_{2+} products become higher, with C_2H_4 stopping being the dominant product and liquid C_{2+} products equaling its Faradaic efficiency.

To assess the effect of silver in the production rate of C_{2+} products as well as on the selectivity towards liquid oxygenates, we electrodeposited pure Cu nanostructures from DES at -1.05 $V_{Ag|AgCl}$ with the same loadings and, carried out CO_2RR. Figures 4SA and 4SB show the Cu nanostructures at -200 mC and -485 mC respectively. The NPs present a flower shape with a diameter close to 300 nm. The size remained the same while the coverage of the deposit clearly increased from -200 mC to -485 mC. This morphology is in good agreement with previous works on Cu electrodeposition from DES in GC.[57] Similarly to the 3Cu:1Ag, the Pb UPD current intensity also increases with the loading of the nanostructures. Figure 10SA shows the Pb UPD of the Cu nanostructures. The calculated R and mass loadings are 0.47 and 0.07 g for -200 mC, 0.64 and 0.09 g for -270 mC and, 1.04 and 0.16 g for -485 mC.

Figure 2C illustrates the CO_2RR efficiencies and total intrinsic current densities at the optimal potentials of -1.0 V_{RHE} and -1.1 V_{RHE} of our Cu nanostructures at -485 mC. The values and partial intrinsic currents of each product for the sample at -485 mC are also summarized in Table S5. At both chosen overpotentials, we have observed a huge increase in the H_2 production compared to 3Cu:1Ag nanostructures. A 58% and 66% of H_2 were detected at -1.0 V_{RHE} and -1.1 V_{RHE}, respectively. On the contrary, CO production has decreased to a 4% at -1.0 V_{RHE} while it was mainly negligible at -1.1 V_{RHE}. The faradaic efficiency of ethylene stayed near 8% at both potentials, far from the 16% and 22% from 3Cu:1Ag at -1.1 V_{RHE}. At -1.0 V_{RHE}, we have detected 1 % of acetate and no ethanol, propanol, or ethylene glycol. The main product after H_2 was formate. At -1.1 V_{RHE}, 3 % of ethanol was detected, but propanol or ethylene glycol have not been detected. These efficiency values are far from the efficiency value of 20 % for C_{2+} liquids obtained on the 3Cu:1Ag at -1.1 V_{RHE}. We have noticed that while copper nanostructures prepared at -270 mC and -485 mC have exhibited similar results, the sample at -200 mC has produced no ethanol at -1.1 V_{RHE} and more CO and formate production. We attribute this change in selectivity to a possible dissolution when the coverage is too low. This

can be expected from the poor coverage and different NPs sizes observed from the SEM image at -200 mC before reaction, and the changes in size and morphology of this sample after reaction (Figure S4). Studies on small copper NPs have reported the possible dissolution or redeposition of the copper once the catalyst is in contact with the alkaline electrolyte when there is no potential control or when first applying a reduction potential.[59,60,65]

Our Cu nanostructures have not exhibited a high efficiency towards liquid C_{2+} products; instead, they are selective toward H_2 production. These results could be explained by a high number of edges and/or defect sites which have been proven to promote the formation of H_2 production in comparison with other facets.[66,67] Even though ethylene is the major C_{2+} product obtained on our Cu nanostructures at -485 mC, its faradic efficiency is lower (7.9 %) than in Cu-Ag nanostructures (18% at -485 mC). In contrast, the partial intrinsic current for ethylene in Cu is higher than that on 3Cu:1Ag, whereas the partial currents of the generated C_{2+} products are similar in both Cu and Cu-Ag electrocatalysts. These results suggest that the suppression of the H_2 on Cu-Ag compared to Cu is one key aspect that improves the product selectivity when adding silver to copper. These results are in line with previous reports which suggested that a suppression of the HER induced by a compressive strain effect when silver is added to copper, enhances the product selectivity.[38]

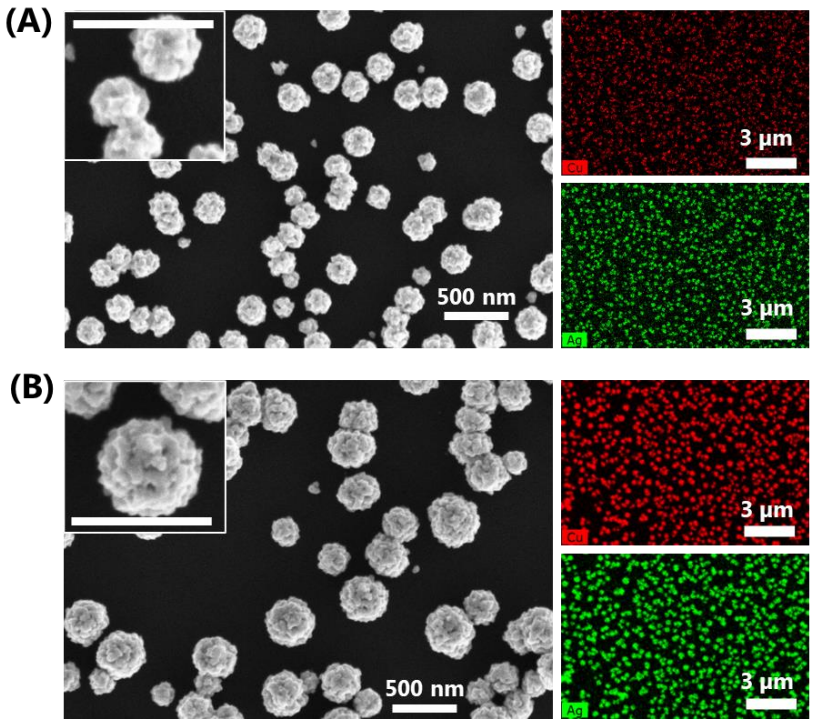

Figure 3. SEM and EDS characterization after 1h of reaction of 3Cu:1Ag at (A) -200 mC and (B) -485 mC. The scale bars on the inlet SEM images correspond to 500 nm.

Figure 3 shows the SEM images and EDS maps of the 3Cu:1Ag nanostructures at -200 mC and -485 mC after one hour of CO_2RR. Neither the morphology nor the composition changed after reaction according to the low-resolution images. Interestingly, despite the high surface diffusion on glassy carbon, we do not observe coalescence or agglomeration of the nanostructures after one hour of reaction. Figures 4SB and 4SD exhibit the SEM images of the Cu samples at -200 mC and -485 mC after one hour of reaction at -1.1 V_{RHE}. The size, shape, and distribution of the NPs remain mainly the same. Even though the NPs did not agglomerate under reaction conditions, we noticed a slightly more rounded shape in the sample at -200 mC which confirms our hypothesis of dissolution and poor stability when the coverage is too low, in agreement with other works.[59,68–70]

To evaluate the changes in the CO_2RR efficiency with the Cu/Ag ratio, we have prepared nanostructures richer in Cu using a 6Cu:1Ag molar ratio bath solution and by applying a potential of -0.73 V_{RHE}. Like the 3Cu:1Ag nanostructures, we have prepared three loadings of

-200 mC, -270 mC, and -485 mC with the 6Cu:1Ag bath composition. Figure 4A shows the SEM image and EDS maps at -485 mC before reaction. The morphology of the NPs has the same rounded shape with porosity as the 3Cu:1Ag. The size is slightly smaller, and the diameter is around 300 nm. The XPS spectra of this sample can also be found in Figure 7SC and 7SD of the S.I, with a surface composition of 1.7:1 of Cu and Ag after 20 seconds of sputtering. The calculated mass loadings based on the EDS results are 0.1 mg for -200 mC, 0.13 mg for -270 mC, and 0.23 mg for -485 mC. Figure 4B shows the SEM and EDS maps after 1 hour of CO_2RR at -1.1 V_{RHE} where the morphology did not change. The EDS analysis shows that the bulk composition varied between 4:1 and 2.5:1 Cu to Ag ratio before (obtained by quantification from EDS color maps from Figure 4A) and after one hour of CO_2RR (color maps from Figure 4B). The SEM images of the 6Cu:1Ag deposits at -200 mC and -270 mC can be found in Figures 5SA and 5SB of the S.I. At lower loadings, the NPs presented the same morphology but a smaller diameter of 200 nm. We have also estimated the ECSA and R of the 6Cu:1Ag nanostructures by Pb-UPD, as shown in Figure 10SB. The ECSA and R from the sample of Figure 4A are 7.48 cm^2 and 1.42, respectively.

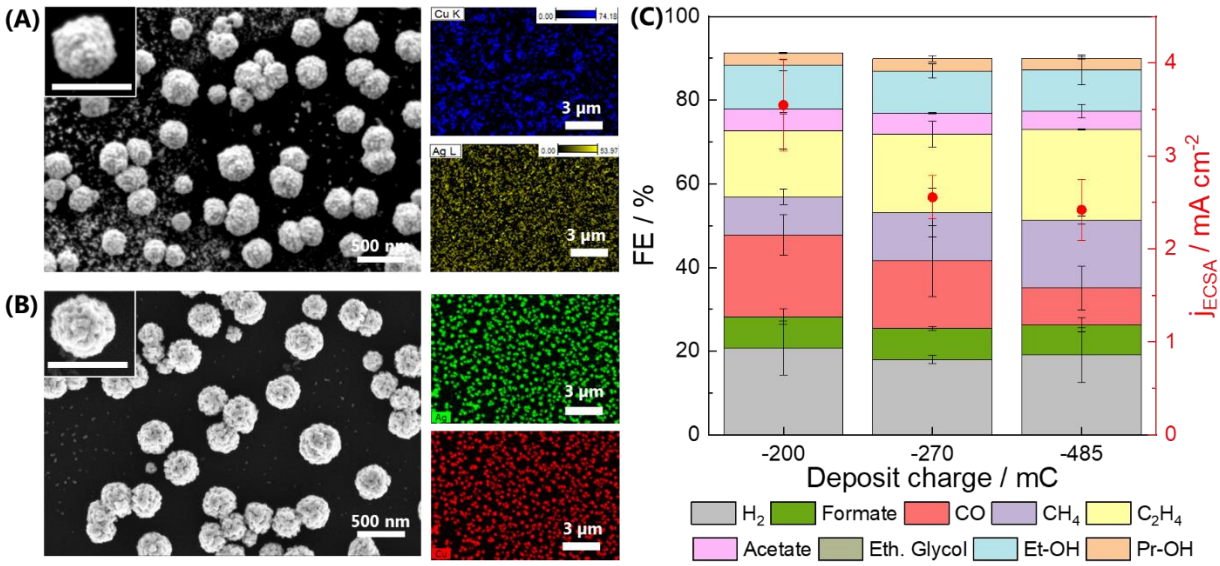

Figure 4. SEM and EDS characterization of 6Cu:1Ag at -485 mC, A) before reaction (EDS at Topsoe), B) after 1h of reaction (EDS at EPFL). The scale bars on the inlet images correspond to 500 nm. C) Product distribution at -1.1V_{RHE} for -200 mC, -270 mV and -485 mC.

Figure 4C exhibits the CO_2RR efficiencies and total intrinsic current density at -1.1 V_{RHE} of the 6Cu:1Ag nanostructures at the three loadings. Tables S6, S7 and S8 in the S.I. show the faradaic efficiency values and partial intrinsic current densities of each product for the -200 mC, -270 mC, and -485 mC, respectively. The results at -1.0 V_{RHE} are illustrated in the S.I. We did not add the results at -1.0 V_{RHE} here since no ethanol, propanol, or ethylene glycol were detected at this potential when the amount of Cu slightly increases on the nanostructure. At -1.1 V_{RHE}, propanol and acetate are detected although ethylene glycol was not detected. This remarks the importance of controlling the Cu/Ag ratio in the nanostructures to increase the production of liquid C_{2+} products over ethylene. Additionally, H_2 remains suppressed between 17 and 21%, similar to the results on 3Cu:1Ag nanostructures. We have also observed that the product selectivity toward CO and CH_4 changes with the loadings. CO decreases with the loadings from 19% to 9% while CH_4 increases from 9% to 16%, approaching more to the behavior of pure copper. We ascribe this fact to that copper electrodeposition is slightly faster than silver for this bath composition, and the amount of copper at the surface may be slightly higher than at lower loading. Ethylene slightly increases as well with the coverage from 15% to 22%. The liquid C_{2+} products represent a 19% to 17% from -200 mC to -485 mC. Ethanol remained the major liquid C_{2+} product with an average of 10%. If we compare these results with the selectivity trends found for the 3Cu:1Ag nanostructures, H_2 remained suppressed, CO became slightly lower, and C_2H_4 and Et-OH were still the major C_{2+} products. We attributed the lower CO and higher C_2H_4 values to the lower silver content. The 6Cu:1Ag deposits behave more similar to pure copper in which it was proven that less CO is available, and ethylene is the most favored C_{2+} product.[18,25,29,36]

4. Discussion of the results:

In this section, we aim to gain a deeper understanding on the structure-activity-selectivity relations and assess the effect of silver on our nanostructures. Figure 5 shows an overview of the partial intrinsic current densities, *i.e.*, the current densities in relation to the number of active surface sites (normalized by the ECSA), of 3Cu:1Ag, 6Cu:1Ag and pure Cu at -485 mC after one hour of CO_2RR at -1.1 V_{RHE}. Figure 5A shows C_2H_4 versus the rest of the liquid C_{2+} products. When adding silver, the ethylene partial current starts to decrease since the surface stops behaving like pure Cu, which promotes ethylene production. Cu-Ag facilitates the pathway towards the formation of liquid alcohols and oxygenates.[38] Concerning the production of liquid C_{2+} products, there is not a huge change in the intrinsic partial current densities within the different Cu/Ag ratios. Ethanol and acetate intrinsic partial current densities remain close in the 3 samples while propanol is promoted in the samples richer in silver.[16] Figure 5B illustrates the intrinsic partial current densities of all the CO_2RR products and H_2 on the three different Cu and Cu-Ag nanostructures. From Cu nanostructures to 6Cu:1Ag and 3Cu:1Ag, we have noticed a clear suppression of the H_2, an increase of CO, and a decrease of CH_4 and formate. However, the partial current densities of the total production of C_{2+} molecules remain similar in the three deposits. The main effect of adding silver in the copper nanostructures is a suppression of the production of hydrogen. A plausible explanation might be that Ag is sited on the Cu undercoordinated sites, which are attributed to promoting H_2, blocking its production.[29,66] An alternative explanation might be a weakening of the *H adsorption energy by a compressive strain effect induced in Cu when Cu and Ag are mixed. Jaramillo, Bell, and co-workers previously reported that the main effect on their Cu-Ag alloys was the suppression of HER. Additionally, they have not observed an improvement in the C_{2+} products, although multi-carbon oxygenates were favored, in line with our results.[38] We attribute the reduction of CH_4 production to the lower availability of adsorbed *H, necessary

for the hydrogenation of this molecule as it has been already discussed by Hori and co-workers.[64]

The similar intrinsic partial current densities of C_{2+} products for all the samples might indicate that the limiting step that controls the reaction rate to produce C_{2+} products is not affected by the pH or hydrogen production. Instead, it might be related to the formation of a carbon-carbon dimer through the C-C coupling step, as discussed by Koper and co-workers in previous reports.[4,71,72] The dimer is the precursor and common intermediate in the production of ethylene, acetaldehyde, ethanol, and also propanol after the insertion of a CO molecule.[8,12,20,73] Although Ag does not change the partial rates of C_{2+} products formation, likely because it does not substantially affect the carbon-carbon dimerization step energetics, it promotes the pathway toward the formation of alcohols and oxygenates over ethylene. The groups of Calle-Vallejo and Yeo already observed an increase of ethanol over ethylene when adding Ag to Oxide Derived-Cu NW.[36] Sargent and co-workers have also shown a Cu/Ag electrode which destabilizes the ethylene reaction pathway promoting ethanol instead.[8] Interestingly, we can smoothly tailor the product distribution towards ethylene and liquid alcohols by tuning the Cu/Ag ratio in our nanostructures deposited in a deep eutectic solvent. This change in product selectivity could be related with a change in the electronic structure of copper, due to strain or ligand effects induced by silver, which increase the CO coverage and reduce the adsorption of *H thus promoting the formation of oxygenates and alcohols.[35,38] However, it is important to remark that our Cu-Ag nanostructures do not intrinsically enhance the production of C_{2+} products over Cu. Indeed, we notice that the partial current densities of C_{2+} in 3Cu:1Ag slightly decay in comparison to Cu-rich nanostructures, fact that we ascribe to an increased amount of surface Ag sites that do not contribute to reduce CO_2 to hydrocarbons but to produce more CO. We note that the production of CO considerably increases from Cu to 3Cu:1Ag whereas the formate decays, as observed in the inset of Fig. 5B, which suggests an

increase of silver sites over copper sites on the surface and during the reaction. Since the shape and size of the Cu-Ag bimetallic nanostructures have barely changed before and after reaction, we believe there is no significant dissolution or redeposition of the copper when the electrodes are in contact with the electrolyte. However, we have considered this possibility for the pure copper nanostructures as stated above.[65] To address how surface composition and structure might change at each applied potential condition and/or under different reaction times, we will need to carry out in-situ operando surface and spectroscopy characterization techniques.

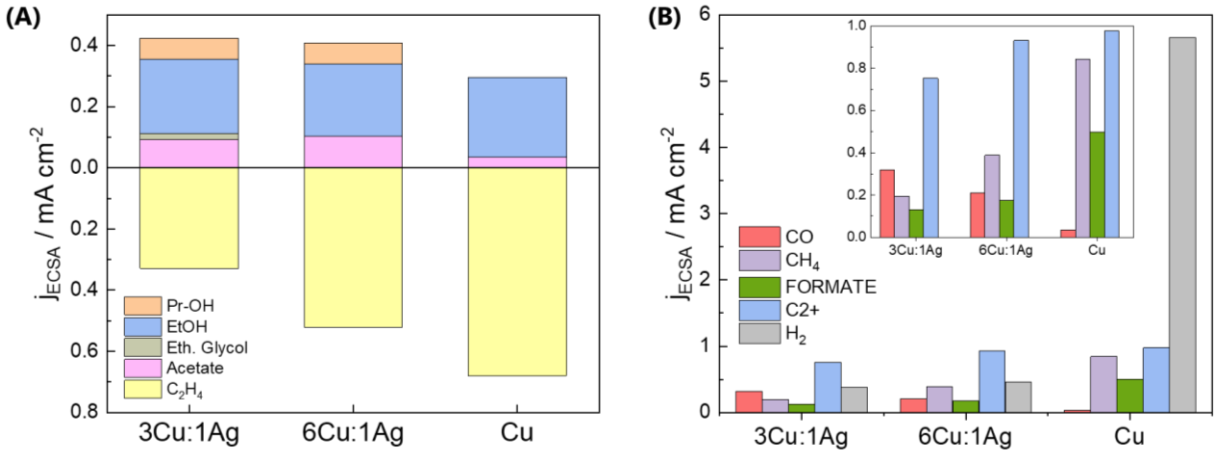

Figure 5. C_{2+} compared with the rest of the products after 1 h of CO_2 reduction at -1.1 V_{RHE}. Products represented against the partial currents normalized by the ECSA for 3Cu:1Ag, 6Cu:1Ag, and Cu at -485 mC.

Our work elucidates the importance of estimating the ECSA to analyze the intrinsic activity of our nanocatalysts under reaction conditions and assess the main effects on selectivity. It is important to remark that the product selectivity and intrinsic activity of our electrodeposited catalysts have been measured in a classical electrochemical H-cell where the amount of dissolved CO_2 that is converted at the electrode surface is low. Recent results on CO_2RR in gas diffusion electrodes (GDEs) have shown that Ag-doped Cu catalysts display a high 80% selectivity toward the formation of C_{2+} with propanol being the major C_{2+} liquid product.[16]

Another recent study on CO_2RR in GDEs has presented Ag-modified Cu oxide-derived catalysts exhibiting up to 90% selectivity for the production of C_{2+} products with ethanol being the major liquid C_{2+} product.[74] Future work using GDEs to investigate the intrinsic partial current densities normalized by the ECSA will be key to elucidate the structure-activity-selectivity relations under realistic conditions of our nanostructures.

5. Conclusions

Herein, we have prepared active Cu-Ag nanostructures with tunable product selectivity for the CO_2RR. We have investigated the performance of our bimetallic nanostructures toward the CO_2RR and addressed how the addition of silver affects the intrinsic partial current density of each product. We highlight the importance of determining the ECSA to report the intrinsic partial activities and decouple the effects of mixing Ag with Cu with those of having different structures in both the selectivity and activity. Our results show that the main improvement in selectivity toward C_{2+} products is due to a suppression of the hydrogen formation on Cu after adding Ag. Although we observe that Ag promotes the formation of alcohols and oxygenates, it does not cause a substantial change in the rate of formation of C_{2+} products. To improve the partial current densities of liquid C_{2+} it would be necessary to prepare CuAg particles with tuned surface structure and large active surface areas.

ORCID

Paula Sebastián-Pascual: 0000-0001-7985-0750

María Escudero-Escribano: 0000-0002-6432-3015

Elena Plaza-Mayoral: 0000-0001-7208-7940

Valery Okatenko: 0000-0002-7542-7995

Kim Nicole Dalby: 0000-0001-6048-3583

Hanne Falsig: 0000-0002-2474-4093

Ib Chorkendorff: 0000-0003-2738-0325

Notes

The authors declare no competing financial interest.

ASSOCIATED CONTENT

A detailed electrochemical characterization of the Cu-Ag electrodeposition from DES by CV and CA analysis is included. The three-electrode glass cell setups for the electrodeposition are also shown. Ex-situ characterization of the Cu and the Cu-Ag nanostructures with SEM images and XPS analysis of the Cu-Ag nanostructures are added. The calculations to determine the mass loadings of all nanostructures by Faraday law are also explained. Additional product distribution analysis after one hour of CO2RR on the 3Cu:1Ag and 6Cu:1Ag are included. Lead UPD voltammograms of the Cu and the 6Cu:1Ag nanostructures have been exhibited

together with a table which summarizes all ECSA and R. Finally, a summary of faradic efficiencies and partial currents of the CO2RR products on different Cu and Cu-Ag nanostructures are included.

ACKNOWLEDGMENT

We acknowledge support from the Danish National Research Foundation Center for High Entropy Alloy Catalysis (CHEAC, DNRF149). We also acknowledge the Villum Foundation for financially supporting this project through a Villum Young Investigator Grant (project number: 19142). This work was also supported by the Danish foundation through the DFF-Research Project1 (Thematic Research, green transition) grant with number: 0217-00213A. PSP gratefully acknowledges the Villum Foundation for its financial support (project number: 53090). VO acknowledges the support from the Swiss National Science Foundation (SNSF) under grant number 200021L_191997/1. This project has also received funding from Villum Fonden V-SUSTAIN (grant number: 9455). We finally acknowledge Prof. Raffaella Buonsanti from EPFL for providing the facilities to perform most of the experiments of this study as well as valuable discussions.

Author contribution:

Elena Plaza-Mayoral: Investigation, Methodology, Formal Analysis, Data curation, Writing - Original Draft, Visualization.

Valery Okatenko: Ex-situ characterization, Investigation, Formal Analysis, Data Curation, Writing - Review & Editing.

Paula Sebastián: Supervision, Methodology, Conceptualization, Writing - Original Draft, Visualization, Project Administration.

Kim Nicole Dalby: Ex-situ characterization, Investigation, Formal Analysis, Data Curation, Writing - Review & Editing.

Hanne Falsig: Resources, Writing - Review & Editing.

Ib Chorkendorff: Data curation, Resources, Writing - Review & Editing.

María Escudero Escribano: Supervision, Methodology, Conceptualization, Writing - Review & Editing, Project Administration, Funding Acquisition.

6. References

[1] K. Calvin, D. Dasgupta, G. Krinner, A. Mukherji, P.W. Thorne, C. Trisos, J. Romero, P. Aldunce, K. Barrett, G. Blanco, W.W.L. Cheung, S. Connors, F. Denton, A. Diongue-Niang, D. Dodman, M. Garschagen, O. Geden, B. Hayward, C. Jones, F. Jotzo, T. Krug, R. Lasco, Y.-Y. Lee, V. Masson-Delmotte, M. Meinshausen, K. Mintenbeck, A. Mokssit, F.E.L. Otto, M. Pathak, A. Pirani, E. Poloczanska, H.-O. Pörtner, A. Revi, D.C. Roberts, J. Roy, A.C. Ruane, J. Skea, P.R. Shukla, R. Slade, A. Slangen, Y. Sokona, A.A. Sörensson, M. Tignor, D. van Vuuren, Y.-M. Wei, H. Winkler, P. Zhai, Z. Zommers, J.-C. Hourcade, F.X. Johnson, S. Pachauri, N.P. Simpson, C. Singh, A. Thomas, E. Totin, A. Alegría, K. Armour, B. Bednar-Friedl, K. Blok, G. Cissé, F. Dentener, S. Eriksen, E. Fischer, G. Garner, C. Guivarch, M. Haasnoot, G. Hansen, M. Hauser, E. Hawkins, T. Hermans, R. Kopp, N. Leprince-Ringuet, J. Lewis, D. Ley, C. Ludden, L. Niamir, Z. Nicholls, S. Some, S. Szopa, B. Trewin, K.-I. van der Wijst, G. Winter, M. Witting, A. Birt, M. Ha, IPCC, 2023: Climate Change 2023: Synthesis Report. Contribution of Working Groups I, II and III to the Sixth Assessment Report of the Intergovernmental Panel on Climate Change [Core Writing Team, H. Lee and J. Romero (eds.)]. IPCC, Geneva, Switzerland., 2023. https://doi.org/10.59327/IPCC/AR6-9789291691647.

[2] P. Sebastián-Pascual, S. Mezzavilla, I.E.L. Stephens, M. Escudero-Escribano,] Review, Structure-sensitivity and electrolyte effects in CO 2 electroreduction: from model studies to applications, n.d.

[3] S.W. Sheehan, R. Buonsanti, Deriving value from CO2: From catalyst design to industrial implementation, Chem Catalysis 1 (2021) 751–753. https://doi.org/10.1016/j.checat.2021.08.010.

[4] Y.Y. Birdja, E. Pérez-Gallent, M.C. Figueiredo, A.J. Göttle, F. Calle-Vallejo, M.T.M. Koper, Advances and challenges in understanding the electrocatalytic conversion of carbon dioxide to fuels, Nat Energy 4 (2019) 732–745. https://doi.org/10.1038/s41560-019-0450-y.

[5] I.E.L. Stephens, K. Chan, A. Bagger, S.W. Boettcher, J. Bonin, E. Boutin, A.K. Buckley, R. Buonsanti, E.R. Cave, X. Chang, S.W. Chee, A.H.M. da Silva, P. de Luna, O. Einsle, B. Endrődi, M. Escudero-Escribano, J. V. Ferreira de Araujo, M.C. Figueiredo, C. Hahn, K.U. Hansen, S. Haussener, S. Hunegnaw, Z. Huo, Y.J. Hwang, C. Janáky, B.S. Jayathilake, F. Jiao, Z.P. Jovanov, P. Karimi, M.T.M. Koper, K.P. Kuhl, W.H. Lee, Z. Liang, X. Liu, S. Ma, M. Ma, H.S. Oh, M. Robert, B.R. Cuenya, J. Rossmeisl, C. Roy, M.P. Ryan, E.H. Sargent, P. Sebastián-Pascual, B. Seger, L. Steier, P. Strasser, A.S. Varela, R.E. Vos, X. Wang, B. Xu, H. Yadegari, Y. Zhou, 2022

roadmap on low temperature electrochemical CO2 reduction, JPhys Energy 4 (2022). https://doi.org/10.1088/2515-7655/ac7823.

[6] S. Nitopi, E. Bertheussen, S.B. Scott, X. Liu, A.K. Engstfeld, S. Horch, B. Seger, I.E.L. Stephens, K. Chan, C. Hahn, J.K. Nørskov, T.F. Jaramillo, I. Chorkendorff, Progress and Perspectives of Electrochemical CO2 Reduction on Copper in Aqueous Electrolyte, Chem Rev 119 (2019) 7610–7672. https://doi.org/10.1021/acs.chemrev.8b00705.

[7] P. Wang, H. Yang, C. Tang, Y. Wu, Y. Zheng, T. Cheng, K. Davey, X. Huang, S.Z. Qiao, Boosting electrocatalytic CO2–to–ethanol production via asymmetric C–C coupling, Nat Commun 13 (2022). https://doi.org/10.1038/s41467-022-31427-9.

[8] Y.C. Li, Z. Wang, T. Yuan, D.H. Nam, M. Luo, J. Wicks, B. Chen, J. Li, F. Li, F.P.G. De Arquer, Y. Wang, C.T. Dinh, O. Voznyy, D. Sinton, E.H. Sargent, Binding Site Diversity Promotes CO2 Electroreduction to Ethanol, J Am Chem Soc 141 (2019) 8584–8591. https://doi.org/10.1021/jacs.9b02945.

[9] K.J.P. Schouten, F. Calle-Vallejo, M.T.M. Koper, A step closer to the electrochemical production of liquid fuels, Angewandte Chemie - International Edition 53 (2014) 10858–10860. https://doi.org/10.1002/anie.201406174.

[10] X. Wang, P. Ou, A. Ozden, S.F. Hung, J. Tam, C.M. Gabardo, J.Y. Howe, J. Sisler, K. Bertens, F.P. García de Arquer, R.K. Miao, C.P. O'Brien, Z. Wang, J. Abed, A.S. Rasouli, M. Sun, A.H. Ip, D. Sinton, E.H. Sargent, Efficient electrosynthesis of n-propanol from carbon monoxide using a Ag–Ru–Cu catalyst, Nat Energy 7 (2022) 170–176. https://doi.org/10.1038/s41560-021-00967-7.

[11] X. Wang, Z. Wang, F.P. García de Arquer, C.T. Dinh, A. Ozden, Y.C. Li, D.H. Nam, J. Li, Y.S. Liu, J. Wicks, Z. Chen, M. Chi, B. Chen, Y. Wang, J. Tam, J.Y. Howe, A. Proppe, P. Todorović, F. Li, T.T. Zhuang, C.M. Gabardo, A.R. Kirmani, C. McCallum, S.F. Hung, Y. Lum, M. Luo, Y. Min, A. Xu, C.P. O'Brien, B. Stephen, B. Sun, A.H. Ip, L.J. Richter, S.O. Kelley, D. Sinton, E.H. Sargent, Efficient electrically powered CO2-to-ethanol via suppression of deoxygenation, Nat Energy 5 (2020) 478–486. https://doi.org/10.1038/s41560-020-0607-8.

[12] D. Gao, R.M. Arán-Ais, H.S. Jeon, B. Roldan Cuenya, Rational catalyst and electrolyte design for CO2 electroreduction towards multicarbon products, Nat Catal 2 (2019) 198–210. https://doi.org/10.1038/s41929-019-0235-5.

[13] I. Ledezma-Yanez, E.P. Gallent, M.T.M. Koper, F. Calle-Vallejo, Structure-sensitive electroreduction of acetaldehyde to ethanol on copper and its mechanistic implications for CO and CO2 reduction, Catal Today 262 (2016) 90–94. https://doi.org/10.1016/j.cattod.2015.09.029.

[14] B. Bian, L. Shi, K.P. Katuri, J. Xu, P. Wang, P.E. Saikaly, Efficient solar-to-acetate conversion from CO2 through microbial electrosynthesis coupled with stable photoanode, Appl Energy 278 (2020). https://doi.org/10.1016/j.apenergy.2020.115684.

[15] Q. Yang, X. Liu, S. Zhu, W. Huang, D. Zhang, Efficient Utilization of CO 2 in a Coal to Ethylene Glycol Process Integrated with Dry/Steam-Mixed Reforming: Conceptual Design and Technoeconomic Analysis, ACS Sustain Chem Eng 7 (2019) 3496–3510. https://doi.org/10.1021/acssuschemeng.8b05757.

[16] X. Wang, Z. Wang, T.T. Zhuang, C.T. Dinh, J. Li, D.H. Nam, F. Li, C.W. Huang, C.S. Tan, Z. Chen, M. Chi, C.M. Gabardo, A. Seifitokaldani, P. Todorović, A. Proppe, Y. Pang, A.R. Kirmani, Y. Wang, A.H. Ip, L.J. Richter, B. Scheffel, A. Xu, S.C. Lo, S.O. Kelley, D. Sinton, E.H. Sargent, Efficient upgrading of CO to C3 fuel using asymmetric C-C coupling active sites, Nat Commun 10 (2019). https://doi.org/10.1038/s41467-019-13190-6.

[17] D.S. Ripatti, T.R. Veltman, M.W. Kanan, Carbon Monoxide Gas Diffusion Electrolysis that Produces Concentrated C2 Products with High Single-Pass Conversion, Joule 3 (2019) 240–256. https://doi.org/10.1016/j.joule.2018.10.007.

[18] M. Wang, V. Nikolaou, A. Loiudice, I.D. Sharp, A. Llobet, R. Buonsanti, Tandem electrocatalytic CO2 reduction with Fe-porphyrins and Cu nanocubes enhances ethylene production, Chem Sci 526 (2022). https://doi.org/10.1039/d2sc04794b.

[19] O. Christensen, S. Zhao, Z. Sun, A. Bagger, J.V. Lauritsen, S.U. Pedersen, K. Daasbjerg, J. Rossmeisl, Can the CO2Reduction Reaction Be Improved on Cu: Selectivity and Intrinsic Activity of Functionalized Cu Surfaces, ACS Catal 12 (2022) 15737–15749. https://doi.org/10.1021/acscatal.2c04200.

[20] K.P. Kuhl, E.R. Cave, D.N. Abram, T.F. Jaramillo, New insights into the electrochemical reduction of carbon dioxide on metallic copper surfaces, Energy Environ Sci 5 (2012) 7050–7059. https://doi.org/10.1039/c2ee21234j.

[21] T. Jaster, A. Gawel, D. Siegmund, J. Holzmann, H. Lohmann, E. Klemm, U.-P. Apfel, iScience Electrochemical CO 2 reduction toward multicarbon alcohols-The microscopic world of catalysts & process conditions, (n.d.). https://doi.org/10.1016/j.isci.

[22] Y. Hori, A. Murata, R. Takahashi, S. Suzuki, Electroreduction of carbon monoxide to methane and ethylene at a copper electrode in aqueous solutions at ambient temperature and pressure, J Am Chem Soc 109 (1987) 5022–5023.

[23] G. Mangione, J. Huang, R. Buonsanti, C. Corminboeuf, Dual-facet mechanism in copper nanocubes for electrochemical CO2 Reduction into Ethylene, Journal of Physical Chemistry Letters 10 (2019) 4259–4265. https://doi.org/10.1021/acs.jpclett.9b01471.

[24] X. Zhao, L. Du, B. You, Y. Sun, Integrated design for electrocatalytic carbon dioxide reduction, Catal Sci Technol 10 (2020) 2711–2720. https://doi.org/10.1039/d0cy00453g.

[25] K. Rossi, R. Buonsanti, Shaping Copper Nanocatalysts to Steer Selectivity in the Electrochemical CO2 Reduction Reaction, Acc Chem Res 55 (2022) 629–637. https://doi.org/10.1021/acs.accounts.1c00673.

[26] R.M. Arán-Ais, F. Scholten, S. Kunze, R. Rizo, B. Roldan Cuenya, The role of in situ generated morphological motifs and Cu(i) species in C2+ product selectivity during CO2 pulsed electroreduction, Nat Energy 5 (2020) 317–325. https://doi.org/10.1038/s41560-020-0594-9.

[27] Y. Hori, I. Takahashi, O. Koga, N. Hoshi, Electrochemical reduction of carbon dioxide at various series of copper single crystal electrodes, J Mol Catal A Chem 199 (2003) 39–47. https://doi.org/10.1016/S1381-1169(03)00016-5.

[28] C.G. Morales-Guio, E.R. Cave, S.A. Nitopi, J.T. Feaster, L. Wang, K.P. Kuhl, A. Jackson, N.C. Johnson, D.N. Abram, T. Hatsukade, C. Hahn, T.F. Jaramillo, Improved CO2 reduction activity

towards C2+ alcohols on a tandem gold on copper electrocatalyst, Nat Catal 1 (2018) 764–771. https://doi.org/10.1038/s41929-018-0139-9.

[29] P. Iyengar, M.J. Kolb, J.R. Pankhurst, F. Calle-Vallejo, R. Buonsanti, Elucidating the Facet-Dependent Selectivity for CO2Electroreduction to Ethanol of Cu-Ag Tandem Catalysts, ACS Catal 11 (2021) 4456–4463. https://doi.org/10.1021/acscatal.1c00420.

[30] S. Ma, M. Sadakiyo, M. Heim, R. Luo, R.T. Haasch, J.I. Gold, M. Yamauchi, P.J.A. Kenis, Electroreduction of carbon dioxide to hydrocarbons using bimetallic Cu-Pd catalysts with different mixing patterns, J Am Chem Soc 139 (2017) 47–50. https://doi.org/10.1021/jacs.6b10740.

[31] H.L.A. Dickinson, M.D. Symes, Recent progress in CO2 reduction using bimetallic electrodes containing copper, Electrochem Commun 135 (2022). https://doi.org/10.1016/j.elecom.2022.107212.

[32] A. Vasileff, C. Xu, Y. Jiao, Y. Zheng, S.Z. Qiao, Surface and Interface Engineering in Copper-Based Bimetallic Materials for Selective CO2 Electroreduction, Chem 4 (2018) 1809–1831. https://doi.org/10.1016/j.chempr.2018.05.001.

[33] D. Ren, B.S.H. Ang, B.S. Yeo, Tuning the Selectivity of Carbon Dioxide Electroreduction toward Ethanol on Oxide-Derived CuxZn Catalysts, ACS Catal 6 (2016) 8239–8247. https://doi.org/10.1021/acscatal.6b02162.

[34] Y. Wang, D. Wang, C.J. Dares, S.L. Marquard, M. V. Sheridan, T.J. Meyer, CO2 reduction to acetate in mixtures of ultrasmall (Cu)n,(Ag)m bimetallic nanoparticles, Proc Natl Acad Sci U S A 115 (2017) 278–283. https://doi.org/10.1073/pnas.1713962115.

[35] Y. Qiao, G. Kastlunger, R.C. Davis, C.A.G. Rodriguez, A. Vishart, W. Deng, Q. Xu, S. Li, P. Benedek, J. Chen, J. Schröder, J. Perryman, D.U. Lee, T.F. Jaramillo, I. Chorkendorff, B. Seger, Mechanistic Insights into Aldehyde Production from Electrochemical CO 2 Reduction on CuAg Alloy via Operando X-ray Measurements , ACS Catal (2023) 9379–9391. https://doi.org/10.1021/acscatal.3c01009.

[36] L.R.L. Ting, O. Piqué, S.Y. Lim, M. Tanhaei, F. Calle-Vallejo, B.S. Yeo, Enhancing CO2 Electroreduction to Ethanol on Copper-Silver Composites by Opening an Alternative Catalytic Pathway, ACS Catal 10 (2020) 4059–4069. https://doi.org/10.1021/acscatal.9b05319.

[37] A. Bagger, W. Ju, A.S. Varela, P. Strasser, J. Rossmeisl, Electrochemical CO2 Reduction: A Classification Problem, ChemPhysChem 18 (2017) 3266–3273. https://doi.org/10.1002/cphc.201700736.

[38] E.L. Clark, C. Hahn, T.F. Jaramillo, A.T. Bell, Electrochemical CO2 Reduction over Compressively Strained CuAg Surface Alloys with Enhanced Multi-Carbon Oxygenate Selectivity, J Am Chem Soc 139 (2017) 15848–15857. https://doi.org/10.1021/jacs.7b08607.

[39] S. Lee, G. Park, J. Lee, Importance of Ag-Cu Biphasic Boundaries for Selective Electrochemical Reduction of CO2 to Ethanol, ACS Catal 7 (2017) 8594–8604. https://doi.org/10.1021/acscatal.7b02822.

[40] H. You, S. Yang, B. Ding, H. Yang, Synthesis of colloidal metal and metal alloy nanoparticles for electrochemical energy applications, Chem. Soc. Rev. 42 (2013) 2880–2904. https://doi.org/10.1039/C2CS35319A.

[41] Y. Tan, X. Xue, Q. Peng, H. Zhao, T. Wang, Y. Li, Controllable fabrication and electrical performance of single crystalline Cu2O nanowires with high aspect ratios, Nano Lett 7 (2007) 3723–3728. https://doi.org/10.1021/nl0721259.

[42] D. Li, C. Wang, D. Tripkovic, S. Sun, N.M. Markovic, V.R. Stamenkovic, Surfactant removal for colloidal nanoparticles from solution synthesis: The effect on catalytic performance, ACS Catal 2 (2012) 1358–1362. https://doi.org/10.1021/cs300219j.

[43] M. Manolova, R. Böck, I. Scharf, T. Mehner, T. Lampke, Electrodeposition of Pd alloys from choline chloride/urea deep eutectic solvents, J Alloys Compd 855 (2021) 157462. https://doi.org/https://doi.org/10.1016/j.jallcom.2020.157462.

[44] R. Bernasconi, G. Panzeri, A. Accogli, F. Liberale, L. Nobili, L. Magagnin, Electrodeposition from Deep Eutectic Solvents, Progress and Developments in Ionic Liquids (2017). https://doi.org/10.5772/64935.

[45] V. S. Protsenko, F.I. Danilov, Current Trends in Electrodeposition of Electrocatalytic Coatings, in: A.A. Inamuddin, Boddula R. (Ed.), Methods for Electrocatalysis. Springer, Chams, 2020.

[46] E. Plaza-Mayoral, I.J. Pereira, K. Nicole Dalby, K.D. Jensen, I. Chorkendorff, H. Falsig, P. Sebastián-Pascual, M. Escudero-Escribano, Pd-Au Nanostructured Electrocatalysts with Tunable Compositions for Formic Acid Oxidation, ACS Appl Energy Mater 5 (2022) 10632–10644. https://doi.org/10.1021/acsaem.2c01361.

[47] P. Sebastián, E. Torralba, E. Vallés, A. Molina, E. Gómez, Advances in Copper Electrodeposition in Chloride Excess. A Theoretical and Experimental Approach, Electrochim Acta 164 (2015) 187–195. https://doi.org/10.1016/j.electacta.2015.02.206.

[48] P. Sebastián, E. Vallés, E. Gómez, First stages of silver electrodeposition in a deep eutectic solvent. Comparative behavior in aqueous medium, Electrochim Acta 112 (2013) 149–158. https://doi.org/10.1016/j.electacta.2013.08.144.

[49] P. Sebastiá, V. Climent, J.M. Feliu, Ionic Liquids in the Field of Metal Electrodeposition, 2018.

[50] S.Z. El Abedin, M. Pölleth, S.A. Meiss, J. Janek, F. Endres, Ionic liquids as green electrolytes for the electrodeposition of nanomaterials, Green Chemistry 9 (2007) 549–55. https://doi.org/10.1039/b614520e.

[51] E. Plaza-Mayoral, K.N. Dalby, H. Falsig, I. Chorkendorff, P. Sebastián-Pascual, M. Escudero-Escribano, Electrodeposition of tuneable Cu-Ag nanostructures in a deep eutectic solvent, ChemRXiv (2024). https://doi.org/10.26434/chemrxiv-2024-lckq9.

[52] E. Plaza-Mayoral, P. Sebastián-Pascual, K.N. Dalby, K.D. Jensen, I. Chorkendorff, H. Falsig, M. Escudero-Escribano, Preparation of high surface area Cu-Au bimetallic nanostructured materials by co-electrodeposition in a deep eutectic solvent, Electrochim Acta 398 (2021) 139309. https://doi.org/10.1016/j.electacta.2021.139309.

[53] P. Sebastián-Pascual, M. Escudero-Escribano, Surface characterization of copper electrocatalysts by lead underpotential deposition, Journal of Electroanalytical Chemistry 896 (2021). https://doi.org/10.1016/j.jelechem.2021.115446.

[54] E. Herrero, L.J. Buller, H.D. Abruña, Underpotential deposition at single crystal surfaces of Au, Pt, Ag and other materials, Chem Rev 101 (2001) 1897–1930. https://doi.org/10.1021/cr9600363.

[55] P. Sebastián, E. Vallés, E. Gómez, Copper electrodeposition in a deep eutectic solvent. First stages analysis considering Cu(I) stabilization in chloride media, Electrochim Acta 123 (2014) 285–295. https://doi.org/10.1016/j.electacta.2014.01.062.

[56] P. Lobaccaro, M.R. Singh, E.L. Clark, Y. Kwon, A.T. Bell, J.W. Ager, Effects of temperature and gas-liquid mass transfer on the operation of small electrochemical cells for the quantitative evaluation of CO2 reduction electrocatalysts, Physical Chemistry Chemical Physics 18 (2016) 26777–26785. https://doi.org/10.1039/c6cp05287h.

[57] P. Sebastián, E. Vallés, E. Gómez, Copper electrodeposition in a deep eutectic solvent. First stages analysis considering Cu(I) stabilization in chloride media, Electrochim Acta 123 (2014) 285–295. https://doi.org/10.1016/j.electacta.2014.01.062.

[58] H. Liao, A. Fisher, Z.J. Xu, Surface Segregation in Bimetallic Nanoparticles: A Critical Issue in Electrocatalyst Engineering, Small 11 (2015) 3221–3246. https://doi.org/10.1002/smll.201403380.

[59] D. Hochfilzer, J.E. Sørensen, E.L. Clark, S.B. Scott, I. Chorkendorff, J. Kibsgaard, The Importance of Potential Control for Accurate Studies of Electrochemical CO Reduction, ACS Energy Lett 6 (2021) 1879–1885. https://doi.org/10.1021/acsenergylett.1c00496.

[60] J. Vavra, T.H. Shen, D. Stoian, V. Tileli, R. Buonsanti, Real-time Monitoring Reveals Dissolution/Redeposition Mechanism in Copper Nanocatalysts during the Initial Stages of the CO2 Reduction Reaction, Angewandte Chemie - International Edition 60 (2021) 1347–1354. https://doi.org/10.1002/anie.202011137.

[61] S. Trasatti, O.A. Petrii, Real surface area measurements in electrochemistry, J. Electroanal. Chem 327 (1992) 353–376. https://doi.org/10.1016/0926-860X(96)80148-7.

[62] D. Li, C. Batchelor-McAuley, R.G. Compton, Some thoughts about reporting the electrocatalytic performance of nanomaterials, Appl Mater Today 18 (2020) 1–6. https://doi.org/10.1016/j.apmt.2019.05.011.

[63] H. Zhang, X. Chang, J.G. Chen, W.A. Goddard, B. Xu, M.J. Cheng, Q. Lu, Computational and experimental demonstrations of one-pot tandem catalysis for electrochemical carbon dioxide reduction to methane, Nat Commun 10 (2019). https://doi.org/10.1038/s41467-019-11292-9.

[64] Y. Hori, A. Murata, R. Takahashi, Formation of hydrocarbons in the electrochemical reduction of carbon dioxide at a copper electrode in aqueous solution, Journal of the Chemical Society, Faraday Transactions 1: Physical Chemistry in Condensed Phases 85 (1989) 2309–2326. https://doi.org/10.1039/F19898502309.

[65] R.M. Arán-Ais, R. Rizo, P. Grosse, G. Algara-Siller, K. Dembélé, M. Plodinec, T. Lunkenbein, S.W. Chee, B. Roldan Cuenya, Imaging electrochemically synthesized Cu2O cubes and their morphological evolution under conditions relevant to CO2 electroreduction, Nat Commun 11 (2020). https://doi.org/10.1038/s41467-020-17220-6.

[66] P. Kratzer, B. Hammer, J.K. Norskov, Geometric and electronic factors determining the differences in reactivity of H2 on Cu(100) and Cu(111), 1996.

[67] R. Reske, H. Mistry, F. Behafarid, B. Roldan Cuenya, P. Strasser, Particle size effects in the catalytic electroreduction of CO2 on Cu nanoparticles, J Am Chem Soc 136 (2014) 6978–6986. https://doi.org/10.1021/ja500328k.

[68] S. Popović, M. Smiljanić, P. Jovanovič, J. Vavra, R. Buonsanti, N. Hodnik, Stability and Degradation Mechanisms of Copper-Based Catalysts for Electrochemical CO2 Reduction, Angewandte Chemie - International Edition 59 (2020) 14736–14746. https://doi.org/10.1002/anie.202000617.

[69] J. Huang, N. Hörmann, E. Oveisi, A. Loiudice, G.L. De Gregorio, O. Andreussi, N. Marzari, R. Buonsanti, Potential-induced nanoclustering of metallic catalysts during electrochemical CO2 reduction, Nat Commun 9 (2018). https://doi.org/10.1038/s41467-018-05544-3.

[70] R.M. Arán-Ais, D. Gao, B. Roldan Cuenya, Structure- and Electrolyte-Sensitivity in CO2 Electroreduction, Acc Chem Res 51 (2018) 2906–2917. https://doi.org/10.1021/acs.accounts.8b00360.

[71] R. Kortlever, J. Shen, J.P. Schouten, F. Calle-Vallejo, M.T.M. Koper, Catalysts and Reaction Pathways for the Electrochemical Reduction of Carbon Dioxide, 2015. http://pubs.acs.org.

[72] K.J.P. Schouten, Y. Kwon, C.J.M. Van Der Ham, Z. Qin, M.T.M. Koper, A new mechanism for the selectivity to C1 and C2 species in the electrochemical reduction of carbon dioxide on copper electrodes, Chem Sci 2 (2011) 1902–1909. https://doi.org/10.1039/c1sc00277e.

[73] Y. Zheng, A. Vasileff, X. Zhou, Y. Jiao, M. Jaroniec, S.Z. Qiao, Understanding the Roadmap for Electrochemical Reduction of CO2 to Multi-Carbon Oxygenates and Hydrocarbons on Copper-Based Catalysts, J Am Chem Soc 141 (2019) 7646–7659. https://doi.org/10.1021/jacs.9b02124.

[74] J. Li, H. Xiong, X. Liu, D. Wu, D. Su, B. Xu, Q. Lu, Weak CO binding sites induced by Cu–Ag interfaces promote CO electroreduction to multi-carbon liquid products, Nat Commun 14 (2023). https://doi.org/10.1038/s41467-023-36411-5.